AIAA 2002−0139

Influence of Humps and Steps on the Stability Characteristics of a 2D Laminar Boundary Layer

A. Wörner, U. Rist and S. Wagner

Institut für Aerodynamik und Gasdynamik
Universität Stuttgart
Stuttgart, Germany

40th AIAA Aerospace Sciences Meeting & Exhibit
14−17 January 2002 / Reno, NV

AIAA 2002-0139

INFLUENCE OF HUMPS AND STEPS ON THE STABILITY CHARACTERISTICS OF A 2D LAMINAR BOUNDARY LAYER

Anke Wörner* , **Ulrich Rist**† and **Siegfried Wagner** ‡
Institut für Aerodynamik und Gasdynamik, Universität Stuttgart,
Pfaffenwaldring 21, 70550 Stuttgart, Germany

Abstract

The influence of humps and steps on the stability characteristics of a 2D laminar boundary layer is investigated by means of Direct Numerical Simulations (DNS). The localized surface irregularity is hereby modeled within the cartesian grid by assigning body forces over surfaces that need not coincide with grid lines. Compared to the use of a body fitted coordinate system this method saves memory and computation time. The method is validated by grid refinement tests as well as by a comparison with water channel experiments. The DNS results for the steady flow over a rectangular hump as well as for an instability wave traveling over a hump show a good agreement with the experimental ones. Simulation results show that a localized hump destabilizes the laminar boundary layer, whereas a forward facing step stabilizes it. The destabilization is stronger when the height or the width of the localized hump are increased. A rounded shape of the hump is less destabilizing than a rectangular shape with sharp corners. The parameter which shows the strongest influence on the stability characteristics of the boundary layer is clearly the height of the localized hump.

1 Introduction

The specific fuel consumption of any aircraft is directly related to its drag. A major portion of aircraft drag is due to friction which is confined to the wall boundary layer of the flow. Since a turbulent boundary layer produces higher skin friction than a laminar one, the overall skin friction is highly influenced by the location of laminar-turbulent transition. By means of control (i.e. delay) of laminar-turbulent transition a reduction of the wall friction is possible. A better understanding of the mechanisms of laminar-turbulent transition is the key for being able to actively or passively delay transition on an airfoil.

The process of laminar-turbulent transition can be subdivided into four main stages. The first stage, the so called receptivity, is the penetration of external perturbations into the boundary layer where they are tuned to boundary layer disturbances. The second stage is the linear amplification of these initially created disturbances, the third one is the nonlinear development and the last one the breakdown to turbulence. Within the paper presented here we focus on the influence of surface discontinuities on the stability characteristics of a 2D boundary layer within the linear range of instability.

In the manufacturing process of an airfoil, surface discontinuities such as steps at junctions or small humps are unavoidable. These surface discontinuities can influence the location of transition on the airfoil via two dominating mechanisms.

First, they are possible sources of receptivity, which means that they provide the small length scale which is necessary for the conversion process of large scale external perturbations into small scale boundary layer disturbances (see [1], [2] or [5]). A second aspect is however, that they are also able to either locally stabilize or destabilize the boundary layer.

The study presented here shall provide an insight into the influence of surface irregularities on the amplification of Tollmien-Schlichting waves in a 2D laminar boundary layer. This subject is studied by means of Direct Numerical Simulations (DNS). A similar study was carried out by Gaster & Wang [3]. They experimentally investigated the influence of surface steps on the value of N factors used in estimating the position of transition on airfoils. They found an empirical correlation of experimental mea-

*Research Assistant
†Senior Research Scientist
‡Professor, Member AIAA

surements of transition on a flat plate containing various steps. Within their study it was not possible to distinguish the newly created disturbances by means of receptivity at the step from the change in stability of the boundary layer created by the presence of the step. This is only possible by using numerical simulations where one aspect can be artificially isolated.

2 Numerical Method

The DNS-code used for this investigation is based on a code first developed by Fasel and further improved by Rist, Kloker et al. which is used for the investigation of transition phenomena in a flat plate boundary layer.

2.1 Governing Equations

The DNS are based on the vorticity-velocity formulation of the complete Navier-Stokes equations for incompressible fluids. All spatial scales are nondimensionalized using a reference length $\tilde{L}$ and all velocities using the freestream velocity $\tilde{U}_\infty$, where $\tilde{}$ denotes dimensional variables.

$$\begin{aligned} x &= \frac{\tilde{x}}{\tilde{L}} & u &= \frac{\tilde{u}}{\tilde{U}_\infty} \\ y &= \frac{\tilde{y}}{\tilde{L}} & v &= \frac{\tilde{v}}{\tilde{U}_\infty} \\ t &= \tilde{t}\,\frac{\tilde{U}_\infty}{\tilde{L}} & Re &= \frac{\tilde{U}_\infty \tilde{L}}{\tilde{\nu}} \end{aligned} \qquad (1)$$

Here x denotes the wall-parallel and y the wall-normal direction. u is the velocity parallel to the flat plate, v the wall-normal velocity, t the time, Re the Reynolds number and $\tilde{\nu}$ the kinematic viscosity.

The first step in the numerical calculation is the solution of the vorticity transport equation, which can be written as:

$$\frac{\partial \omega_z}{\partial t} + \frac{\partial}{\partial x}(u \cdot \omega_z) + \frac{\partial}{\partial y}(v \cdot \omega_z) = \frac{1}{Re}\left(\frac{\partial^2 \omega_z}{\partial x^2} + \frac{\partial^2 \omega_z}{\partial y^2}\right) \qquad (2)$$

ω_z denotes the spanwise vorticity, which is defined as:

$$\omega_z = \frac{\partial u}{\partial y} - \frac{\partial v}{\partial x} \qquad (3)$$

Then, the wall-normal velocity v can be calculated by solving the following Poisson-equation:

$$\frac{\partial^2 v}{\partial x^2} + \frac{\partial^2 v}{\partial y^2} = -\frac{\partial \omega_z}{\partial x} \qquad (4)$$

The continuity equation

$$\frac{\partial u}{\partial x} + \frac{\partial v}{\partial y} = 0 \qquad (5)$$

is then used to calculate the wall-parallel velocity u.

2.2 Discretization and Boundary Conditions

The flow field is discretized using fourth-order accurate finite differences in streamwise (x-) and wall-normal (y-) direction on a cartesian grid. A sketch of the integration domain is shown in figure 1. The time integration is done using a fourth order, four step Runge-Kutta scheme. The v-Poisson equation is solved with a multi-grid method, using a vectorizable, stripe-pattern SOR line-iteration technique on each grid. Details concerning the numerical method can be found in [9].

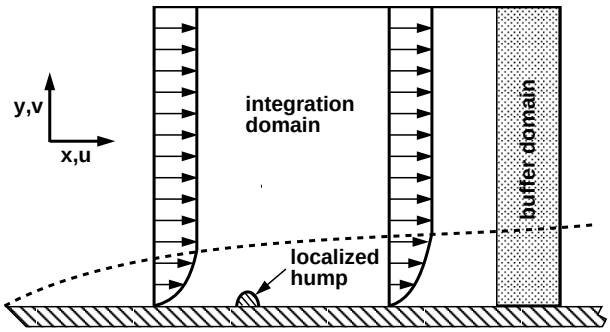

Figure 1: sketch of the integration domain

At the freestream boundary the vorticity is set to zero since this boundary lies in the region of potential flow. For the wall-normal velocity v exponential decay is assumed

$$\frac{\partial v}{\partial y} = -\alpha \cdot v. \qquad (6)$$

Here α denotes a streamwise wavenumber, which is considered to be representative for the whole integration domain. In the potential flow, this condition derives the exact solution for linear TS-waves with the streamwise wave number α.

At the inflow boundary, steady Falkner-Skan profiles, usually Blasius profiles are prescribed.

Disturbances are forced by wall-normal periodic suction and blowing in a disturbance strip at the wall. Except in the disturbance strip, the no-slip and no through-flow condition is applied at the wall.

Upstream of the outflow boundary the unsteady vorticity is smoothly damped to the steady-state value in a buffer domain [6]. Consequently, the unsteady velocity components also decay exponentially in streamwise direction and vanish at the outflow.

2.3 Modeling of the Surface Irregularity

The localized surface irregularity within the cartesian grid is modeled using a technique which is related to Peskin's immersed boundary approach, used for example by Goldstein et al. [4], Linnick [7] or von Terzi et al. [10]. In this approach, the effect of the surface irregularity on the surrounding flow field is modeled with an external force field which enforces no-slip and no-through-flow at selected grid points or at selected points between the grid points at every time step.

The vorticity transport equation for the 2D case with an external force field $\boldsymbol{F} = (F_x, F_y)$ can be written as

$$\begin{aligned} &\frac{\partial \omega_z}{\partial t} + \frac{\partial}{\partial x}(u \cdot \omega_z) \quad + \quad \frac{\partial}{\partial y}(v \cdot \omega_z) \\ &= \frac{1}{Re}\left(\frac{\partial^2 \omega_z}{\partial x^2} + \frac{\partial^2 \omega_z}{\partial y^2}\right) \quad + \quad \frac{\partial F_x}{\partial y} - \frac{\partial F_y}{\partial x}. \end{aligned} \tag{7}$$

The force term on the right hand side is the force exerted by the surface irregularity on the fluid and can be written as

$$\boldsymbol{F} = \oint \boldsymbol{f}(\boldsymbol{x_S}, t) \cdot \delta(\boldsymbol{x} - \boldsymbol{x_S})\, dS. \tag{8}$$

For numerical reasons, the delta function is approximated by a Gaussian function as follows:

$$\delta \approx e^{-\left(\frac{x-x_S}{\sigma_x}\right)^2 - \left(\frac{y-y_s}{\sigma_y}\right)^2} \tag{9}$$

The surface body force $\boldsymbol{f}$ is determined from the relation

$$\boldsymbol{f}(\boldsymbol{x_S}, t) = \alpha \cdot \int_0^t \boldsymbol{v}(\boldsymbol{x_S}, t')\, dt' + \beta \cdot \boldsymbol{v}(\boldsymbol{x_S}, t) \tag{10}$$

for surface points $\boldsymbol{x_S}$, velocity $\boldsymbol{v}$, time t and negative constants α and β which represents a feedback scheme in which the velocity is used to iteratively approach the desired value.

If the surface of the irregularity is located between the grid points, the velocity at this location is interpolated from the values at the neighboring grid points using a 4th order Lagrangian interpolation procedure.

3 Validation

To validate this method of modeling a solid surface within a cartesian grid, the DNS results were compared with experimental results obtained by Lang in the laminar water channel of our institute. Additional grid refinement tests were performed.

3.1 Comparison with Experiments

Figures 2 to 4 show a comparison of the DNS with the water channel experiment of the steady flow over a 2D rectangular hump. The center of the hump is located at $Re_{\delta_1} = 1070$. It's height is $3mm$, it's width $155mm$, giving $h/\delta_1 = 0.37 (Re_H = U_\infty h/\nu = 387)$ and $b/\delta_1 = 19.1$. Plotted is the streamwise velocity u versus y for three different streamwise positions, one at $105mm$ upstream of the center of the hump, one above the hump (at $20mm$ upstream of the center), and one at $120mm$ downstream of the center of the hump, approximately at the location where reattachment takes place.

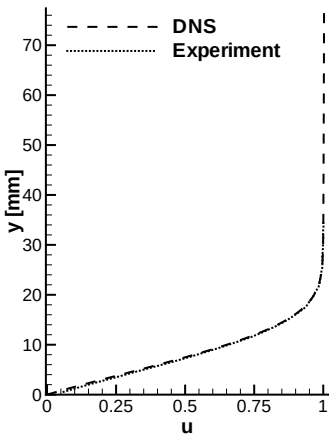

Figure 2: baseflow upstream of the hump; comparison DNS-experiment

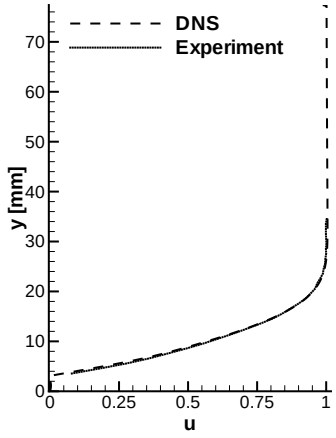

Figure 3: baseflow above the hump; comparison DNS-experiment

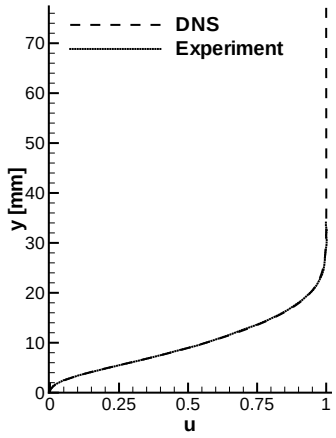

Figure 4: baseflow downstream of the hump; comparison DNS-experiment

The agreement found between the DNS and the experiment is quite good, which proves that the effect of the rectangular hump on the surrounding flow field was correctly modeled by the numerical approach using an external force field.

To investigate whether unsteady effects are also correctly modeled, a second experiment was conducted in the water channel. A TS-wave with a non-dimensional frequency of $F = 2\pi f\nu/U_\infty^2 \cdot 10^6 = 49.34$ and an amplitude of 1% of the freestream velocity U_∞ was created upstream of the hump, using a vibrating ribbon. This TS-wave has a wavelength of $310mm$, which shows that the width of the hump was chosen to be one half of the TS-wavelength. Two different cases were studied. First, the TS-wave traveled along a smooth plate, whereas in a second experiment the TS-wave traveled across the rectangular hump of height $h/\delta_1 = 0.37$, located at $Re_{\delta_1} = 1070$. For both experiments the amplitude profiles of the TS-wave versus y at $535mm$ downstream of the center of the hump were measured.

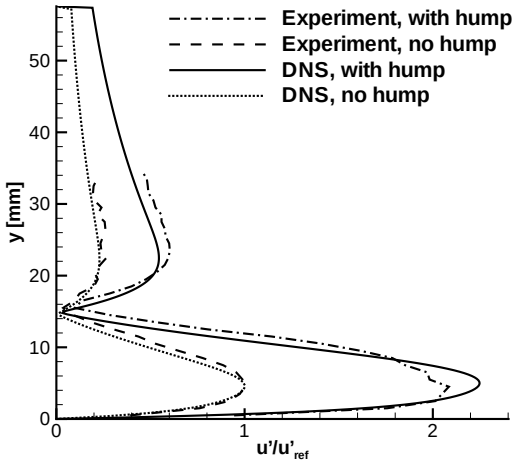

Figure 5: amplitude change of a TS-wave traveling across a rectangular hump; comparison DNS-experiment

Figure 5 compares these amplitude profiles with DNS calculations for the same two cases. In the DNS, the increase in amplitude, which is caused by the presence of the hump, is approximately 7 % higher than in the experiment. This discrepancy can to some extend result from the fact that only a few periods were time-averaged in the experiments and that there were already remarkable 3D disturbances visible in the experiment at this location.

3.2 Grid Refinement Tests

Results of the grid refinement tests are shown in figures 6 and 7. Here amplification curves for a 2D TS-wave traveling across a rectangular hump are shown, which means that the maximum of the amplitude of the streamwise disturbance velocity u' versus y is plotted against the streamwise coordinate x. In figure 6 the streamwise grid spacing is varied, whereas in figure 7 the wall-normal grid spacing is changed.

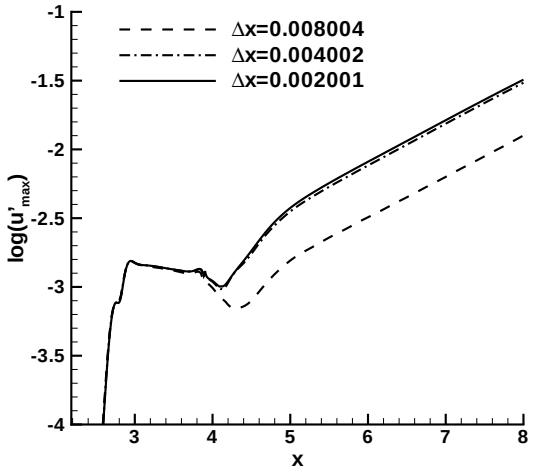

Figure 6: grid refinement tests in x-direction

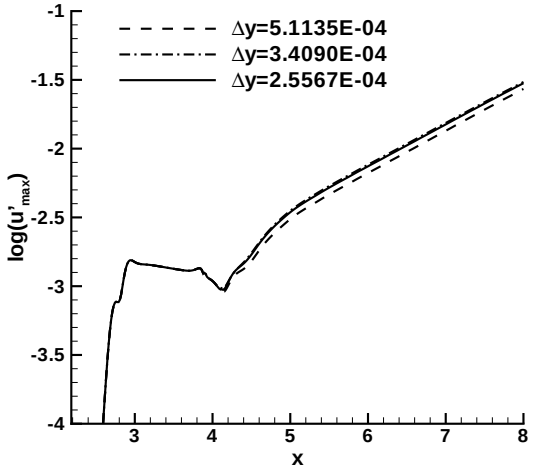

Figure 7: grid refinement tests in y-direction

From these two figures it is clear that the solution converges, and that a resolution of 100 grid points in streamwise direction per TS-wave length($\Delta x = 0.004002$) and 15 grid points in wall-normal direction over the height of the hump($\Delta y = 3.409E-04$) is a sufficient resolution for this problem.

4 Results and Discussion

4.1 Localized Hump

Figure 8 compares the amplification curve for a TS-wave with a non-dimensional frequency $F = 2\pi f\nu/U_\infty^2 \cdot 10^6 = 49.34$ traveling across a rectangular hump located at $x = 4.0$ ($Re_{\delta_1} = 1.72 \cdot \sqrt{Re \cdot x} = 1088; Re = 10^5$) to a TS-wave traveling along a flat plate without any surface irregularities. The height of the hump was 0.47 normalized with the local boundary layer displacement thickness δ_1, which corresponds to $Re_H = U_\infty h/\nu = 511$, and its width was about one half of the wavelength of the TS-wave ($b = 0.1$). The disturbance strip for the creation of the TS-wave was located at $x = 2.78(Re_{\delta_1} = 907)$.

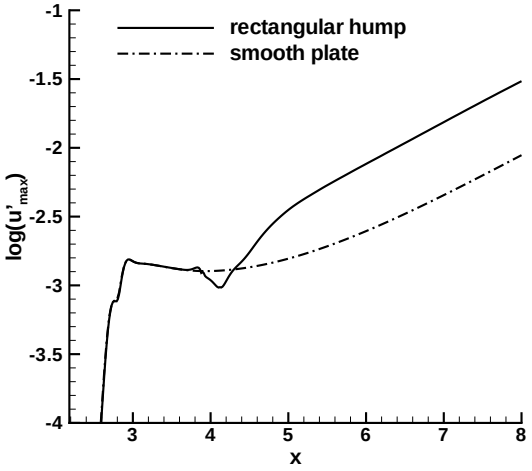

Figure 8: amplitude development of a TS-wave traveling across a rectangular hump located at $x = 4.0$

The influence of the hump on the TS-wave traveling across it can be subdivided into two local effects which finally add up to the global effect of the hump on the TS-wave far downstream of the localized hump. The local effects can be described as follows: First, at the rising edge of the hump, the amplitude of the TS-wave decreases because of the thinner boundary layer that develops at the beginning of the hump. Second, at the falling edge of the hump the amplification of the TS-wave is remarkably increased compared to the wave traveling along a smooth plate. This second effect probably results from a small separation zone which forms behind the rectangular hump. Since the increase in amplification at the falling edge is stronger than the stabilizing effect that occurs at the rising edge, the global effect of a localized hump is a destabilization of the boundary layer. In the case shown in figure 8 the resulting amplitude of the TS-wave far downstream of the hump is about a factor of 3.2 higher

than the amplitude of the TS-wave traveling along a smooth plate.

Several parameters of the rectangular hump are now varied to show their influence on the amplitude development of the TS-wave that travels across the hump.

Influence of Height. First, the varying parameter was the height of the rectangular hump, which was changed between $h/\delta_1 = 0.235$ ($Re_H = 256$) and $h/\delta_1 = 0.94$ ($Re_H = 1023$). All other parameters were kept constant. As expected, the highest hump has the largest influence on the TS-wave, traveling across it. The amplitude of the TS-wave far downstream of the hump increases by a factor of 1.4 for $Re_H = 256$, 3.2 for $Re_H = 511$ and 26.0 for $Re_H = 1023$ by the presence of the hump. This shows that up to a height of $Re_H = 511$ the increase in amplitude of the TS-wave scales approximately linear with the height of the rectangular hump. For $Re_H = 1023$ this dependence becomes nonlinear because the stability characteristics of the boundary layer are dramatically changed. Another hint for this large change in the stability characteristics is the completely different slope of the amplification curve downstream of the hump, compared to the cases with smaller humps.

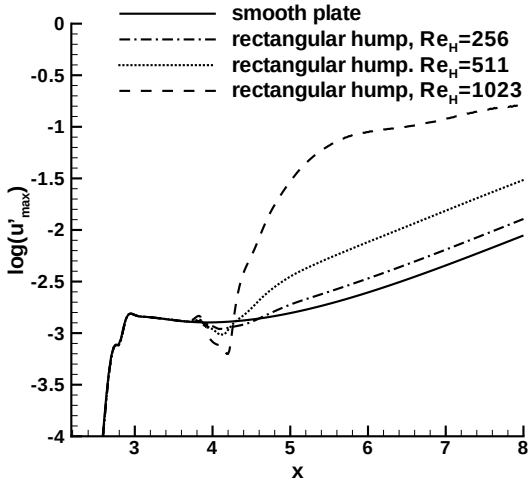

Figure 9: influence of the height of the hump

Influence of Width. Then, the width of the rectangular hump is changed. The results of this variation can be found in figure 10. The width was varied between $b = 0.1$ and $b = 0.4$, the wavelength of the TS-wave is approximately $\lambda_{TS} = 0.2$. The height was $h/\delta_1 = 0.47$ ($Re_H = 511$). The largest influence on the TS-wave is observed for the hump with the largest width. Nevertheless, the parameter that has the most influence on the amplitude increase of the TS-wave is clearly the height of the hump, the width of the hump plays only a minor role.

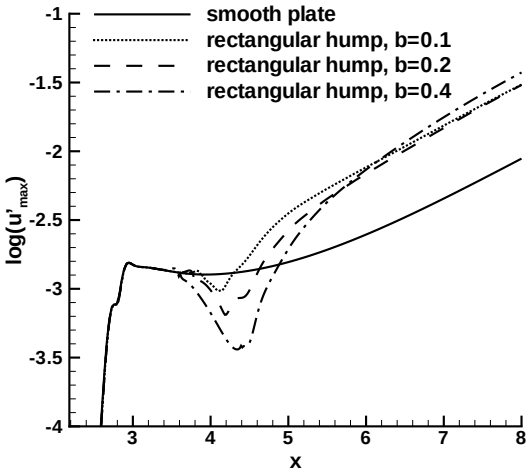

Figure 10: influence of the width of the hump

Influence of Shape. In figure 11 the amplitude development of three TS-waves can be observed. One travels over a rectangular hump, one over a rounded hump, the shape of which is a quadratic function of x, and one travels over a smooth plate. The height of both humps is $h/\delta_1 = 0.47$ ($Re_H = 511$), the width is $b = 0.1$. The rectangular hump with its sharp corners has, as could be expected, the most influence on the stability characteristic of the boundary layer.

4.2 Forward Facing Step

Figure 12 shows the amplification curve for a TS-wave traveling across a forward facing step compared to a TS-wave traveling along a perfectly smooth flat plate. The non-dimensional frequency is the same as before. The forward facing step is located at $x = 4.0$ which corresponds to $Re_{\delta_1} = 1088$. It's height normalized with δ_1 is 0.235 ($Re_H = 256$).

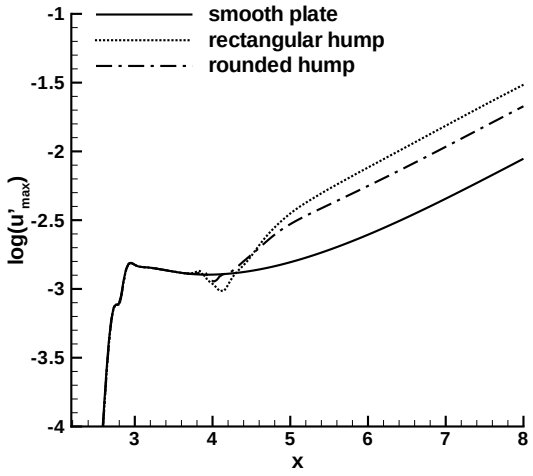

Figure 11: influence of the shape of the hump

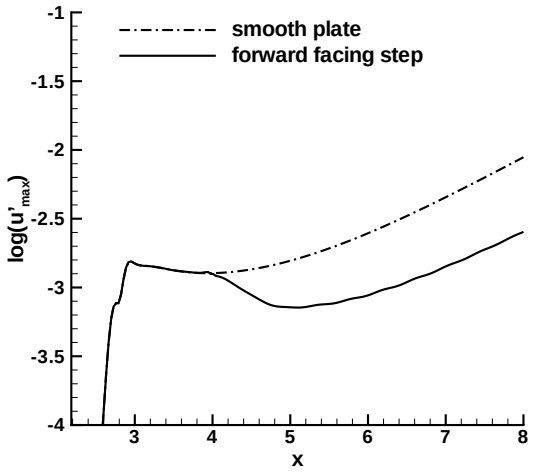

Figure 12: amplitude development of a TS-wave traveling across a forward facing step located at $x = 4.0$

As can be seen, the amplitude of the TS-wave is now reduced by the forward facing step because the thinner boundary layer evolving on the step is more stable than the boundary layer on the smooth plate. The separation zone in front of the step is very small and has therefore merely no influence on the TS-wave. This reduction in amplitude seems surprising, but results from the fact that freestream disturbances are absent in the simulation. This means that no receptivity can take place which in reality would add additional disturbances.

5 Conclusions and Outlook

By means of direct numerical simulations, the influence of humps and steps on the stability characteristics of a 2D laminar boundary layer has been investigated. The localized surface irregularity was modeled within a cartesian grid using an immersed boundary technique, where the influence of a solid wall on the surrounding flow field is modeled by using an external force field which enforces no-slip and no through-flow on the solid wall. This approach was validated by comparing the DNS results with measurements conducted in the laminar water tunnel of our institute. For a steady as well as an unsteady test case, the DNS results were in good agreement with the experimental results. This showed that the effect of a localized hump on the surrounding flow field was correctly modeled by the immersed boundary technique.

A localized hump was found to have an overall destabilizing effect on the laminar boundary layer, whereas a forward facing step showed a stabilizing effect. The destabilization of the boundary layer by the presence of a hump results from the combination of two local phenomena. The TS-wave is first damped by the stabilizing effect of the rising edge of the hump with it's thinner boundary layer, as it can be also seen for the forward facing step. At the falling edge of the hump the amplification is locally highly increased by the presence of a small separation zone behind the hump. This increase in amplification is much stronger than the damping caused by the rising edge of the hump. Therefore, the overall effect of a localized hump is a destabilization of the boundary layer. For the localized hump, the influence of several parameters on the destabilization was investigated. Up to a height, normalized with the local displacement thickness, of approximately $h/\delta_1 = 0.5$ the increase in amplitude of a TS-wave traveling across the hump was found to depend linearly on the height of the hump. For a height of $h/\delta_1 = 0.97$ this dependence was clearly nonlinear. If the width of the hump was increased, the effect on the TS-wave was also found to be larger, but the influence of the width was weaker than the influence of the height of the hump. Additionally, the shape of the hump was varied. A rectangular hump with sharp corners showed a larger influence on the amplitude development of a TS-wave than a rounded hump, the shape of which was a quadratic function of x.

In the future, the immersed boundary technique is planned to be used for numerical simulations of roughness acoustic receptivity. Additionally, the

approach will be extended to be able to deal with 3D surface irregularities.

Acknowledgments

The authors would like to thank M. Lang for the experiments he performed in the laminar water channel to validate the DNS code and the Deutsche Forschungsgemeinschaft (DFG) for the financial support under contracts Ri 680/7-1 and Ri 680/7-2 as a part of the Verbundschwerpunktprogramm Transition.

References

[1] Choudhari, M. and Streett, C.L.: **A finite Reynolds-number approach for the prediction of boundary-layer receptivity in localized regions.** *Phys. Fluids*, A **4**, pp. 2495-2514, (1992).

[2] Crouch, J.D.: **Localized receptivity of boundary layers.** *Phys. Fluids*, A **4**, pp. 1408-1414, (1992)

[3] Gaster, M. and Wang, X.: **The influence of surface steps on the value of 'N' factors used in estimating the position of transition on aerofoils.** *EUROMECH Colloquium 423*, Boundary-Layer Transition in Aerodynamics, 2.-4. April 2001, Stuttgart, (2001).

[4] Goldstein, D., Handler, R. and Sirovich, L.: **Modeling a no-slip flow boundary with an external force field.** *J. Comp. Physics*, 105, pp. 354-366, (1993).

[5] Goldstein, M.E.: **Scattering of acoustic waves into Tollmien-Schlichting waves by small streamwise variations in surface geometry.** *J. Fluid Mech.*, Vol. 154, pp. 509-529, (1985).

[6] Kloker, M., Konzelmann, U. and Fasel, H.: **Outflow boundary conditions for spatial Navier-Stokes simulations of transitional boundary layers.** *AIAA J.*, 31(4), pp. 620-628, (1993).

[7] Linnick, M. N.: **Investigation of actuators for use in active flow control.** M. Sc. Report, University of Arizona, (1999).

[8] Peskin, C.S.: **Numerical analysis of blood flow in the heart.** *J. Comp. Physics*, 25, pp. 220-252, (1977).

[9] Rist, U. and Fasel, H.: **Direct numerical simulation of controlled transition in a flat-plate boundary layer.** *J. Fluid Mech.*, Vol. 298, pp. 211–248, (1995).

[10] von Terzi, D.A., Linnick, M.N., Seidel, J. and Fasel, H.: **Immersed Boundary Techniques for High-Order Finite-Difference Methods.** *AIAA–Paper 2001-2918*, (2001).